Development Characteristics and Dynamic Structure of Tropical Intraseasonal Convection Anomalies*

HUALAN RUI** AND BIN WANG

Department of Meteorology, University of Hawaii, Honolulu, Hawaii

(Manuscript received 29 November 1988, in final form 30 August 1989)

ABSTRACT

The development and dynamical structure of intraseasonal low-frequency convection anomalies in the equatorial region are investigated using 10 years (1975–85) of outgoing longwave radiation (OLR) and 7 years (1979–85) of 200 and 850 mb wind data.

The composite OLR anomalies for 36 cases show a four-stage development process: initiation over equatorial Africa, rapid intensification when passing through the Indian Ocean, mature evolution characterized by a weakening in the maritime continent and redevelopment over the western Pacific, and dissipation near the date line in moderate events or emanation from the equator toward North America and southeastern Pacific in strong events.

A noticeable feature in vertical structure is that the 850 mb convergence leads convection and midtropospheric upward motion by about 30 degrees longitude in both developing and mature phases. Equatorial upper- (lower-) level easterly (westerly) anomalies and associated twin anomalous anticyclonic (cyclonic) circulation anomalies couple with equatorial convection anomalies. The wind anomalies, however, generally lag convection anomalies in development and early mature phases, but nearly overlap in late mature phase and slightly lead the convection anomalies in dissipation phase. The upper-level twin cyclonic cells associated with the westerly anomalies in front of the convection travel across eastern Pacific after the convection ceases in the central Pacific, while the low-level wind anomalies die out east of the date line.

The implications of the findings in relation to theoretical hypotheses on low-frequency motion are discussed.

1. Introduction

The intraseasonal oscillation is a major component of low-frequency variations of the tropical general circulation and has drawn much attention in the last decade. A large number of studies have provided important insights into the mean behavior of the oscillation using correlative or spectral/cross spectral analyses and various versions of principal component analysis. Our starting point is based on the following hypothesis, first conjectured by Madden and Julian (1972): The equatorial intraseasonal oscillation is, to a large extent, caused by systematic eastward movement of low-frequency large-scale convection and circulation anomalies. We regard these anomalies as real dynamic systems. From a dynamical point of view, it is more meaningful to investigate the behavior of individual events directly from time–space domain using relatively raw data (similar to some kind of weather map).

Our study focuses on two important aspects of the equatorial eastward-moving intraseasonal mode: the development and dynamic structure. Many questions regarding the development of this mode remain unanswered. For instance, where do the anomalies form or become identifiable? Is there any evidence of rapid development? How large is the rate of intensification and what are preferred regions for the development and dissipation, if any? How is the development related to basic environmental circulation conditions? Conventional correlative, cross-spectral, or empirical orthogonal function (EOF) analyses have difficulties in describing characteristics in their formative, developmental, mature and dissipative stages. Examination of development from a composite analysis of individual events is expected to provide useful physical insights into the dynamics of the phenomenon.

One of the foci in recent studies of the intraseasonal oscillation is documentation of the structure of the oscillation mode. This is no doubt of central importance for understanding the dynamics of intraseasonal oscillations. Unfortunately, these studies have yielded diverse conclusions. Using composite station wind and OLR data, Madden (1986) proposed a schematic description of upper tropospheric horizontal disturbance structure at the time of large amplitude. His pictures showed that eastward-moving regions of enhanced

* Contribution No. 88-16, Department of Meteorology, University of Hawaii.

** Present affiliation: Department of Meteorology, University of Maryland, College Park, Maryland.

Corresponding author address: Dr. Bin Wang, Department of Meteorology, University of Hawaii, 2525 Corea Road, Honolulu, HI 96822.

© 1990 American Meteorological Society

convection force a Kelvin-like wave to the east and anticyclonic, Rossby-like waves to the west. He emphasized asymmetric response in solstice seasons: the dominant anticyclonic eddies occurring in the summer hemisphere. On the other hand, based on EOF analysis of National Meteorological Center (NMC) wind data and OLR data, Knutson and Weickmann (1987) found anomalous upper tropospheric cyclones to the east of the convection and anticyclones alongside or west of the convection. They emphasized that while convection anomalies are most pronounced in summer hemisphere tropics, the tropical and subtropical rotational flow features are most prominent in the winter hemisphere. Finally, Murakami (1987, 1988) investigated the teleconnection patterns during the eastward propagation phase. He indicated that a succession of upper-level cyclonic and anticyclonic disturbances develop over both northern and southern subtropics mainly downstream of the convection anomalies, while at 850 mb, strong 30–60 day meridional wind anomalies surge from cold midlatitudes. The diverse results invite further study. We present a complimentary analysis using a different compositing procedure and relatively raw data. The results provide additional and more detailed information which is particularly useful in evaluating the relevance of current theoretical hypotheses on the nature of tropical intraseasonal oscillations.

In the next section, the data and composite procedures are briefly described. Section 3 presents composite evolution for 36 events. In sections 4 and 5, horizontal and vertical structures are composed and analyzed for 6 strong cases. The last section summarizes our major findings and discusses their implications in relation to the current theoretical hypotheses.

2. Data and event-composite procedure

a. The data

The area for this study covers the global tropics and subtropics between 45°S and 45°N. Two datasets are used: 1) daily OLR data from National Oceanic and Atmospheric Administration (NOAA) polar orbiting satellites at 2.5° latitude/longitude resolution for 10 years from 1975 to 1985 (no data in 1978), and 2) daily wind data at 200 mb and 850 mb, which were extracted from the objectively analyzed dataset prepared by the European Centre for Medium-range Weather Forecasts (ECMWF) with the same resolution as the OLR field for the period from 1979 through 1985. For the purpose of studying planetary scale low-frequency motions, a nine grid point weighted average was employed to reduce resolution from 2.5° × 2.5° to 5.0° × 5.0°, so that low resolution data contain information from all higher resolution grids.

Normal annual cycle was determined by the sum of the annual mean and the first three harmonics of mean daily data. Subtracting the normal annual cycle from original daily data yields a daily anomaly. The interannual variation was estimated by 3-month weighted mean anomaly (Wang and Murakami 1988). After removing the interannual variation from the daily anomaly, we computed the 5-day mean anomaly which describes primarily the intraseasonal variations with time scale roughly from 10 days to 3 months. The 5-day mean anomalies are used in this study and simply called anomalies. We shall interpret a negative OLR anomaly as a positive convection anomaly in the deep tropics.

b. Selection and stratification of equatorial eastward propagating events

Previous studies selected events based on either zonal wind at a particular station (e.g., Madden 1986) or the first two EOF components (e.g., Knutson and Weickmann 1987; Murakami 1987). We select significant events using both pentad mean anomaly (PMA) maps and Hovmoller diagrams for OLR. PMA OLR averaged between 7.5°S and 7.5°N are displayed in longitude vs. time format in Fig. 1. Since the majority of equatorial convection events occur in the eastern hemisphere, the domain in Fig. 1 does not include tropical America and the Atlantic Ocean. In Fig. 1, each event of eastward propagation is depicted by a negative OLR anomaly band enclosed by -5 W m^{-2} contour and tilted downward and eastward. An ideal persistent eastward propagation corresponds to a continuous band without a gap (discontinuity). If a band structure has a zonal dimension longer than 100° longitude and is nearly continuous with a single gap whose length is less than 15% of the total length of the band structure (but no positive contour in the gap), it is still considered as representing a single event. For convenience, we refer to the continuous or near-continuous band structure as "event-band."

To avoid vagueness and arbitrariness in selecting events, we designed objective criteria in terms of Fig. 1. Four parameters were used to characterize each event. They describe total longitudinal displacement, convective intensity, average duration of convection at fixed longitude, and persistency in eastward movement. The total longitudinal displacement is measured by the longitudinal extent of the event-band (rounded to the nearest 10°); the convective intensity is expressed by the minimum OLR contour value within the event-band; and the averaged duration of convection at fixed longitude is estimated by the average width of the event-band in units of pentad. The degree of persistence in eastward movement depends on the longitudinal length of the single gap (possibly) contained within the event-band (rounded to the nearest 5°). We then converted the values of the above four parameters to scores ranging from 1 to 4 according to Table 1. The sum of these four scores was defined as the intensity index of the event. Each equatorial eastward propagation event was then stratified according to their intensity index: strong

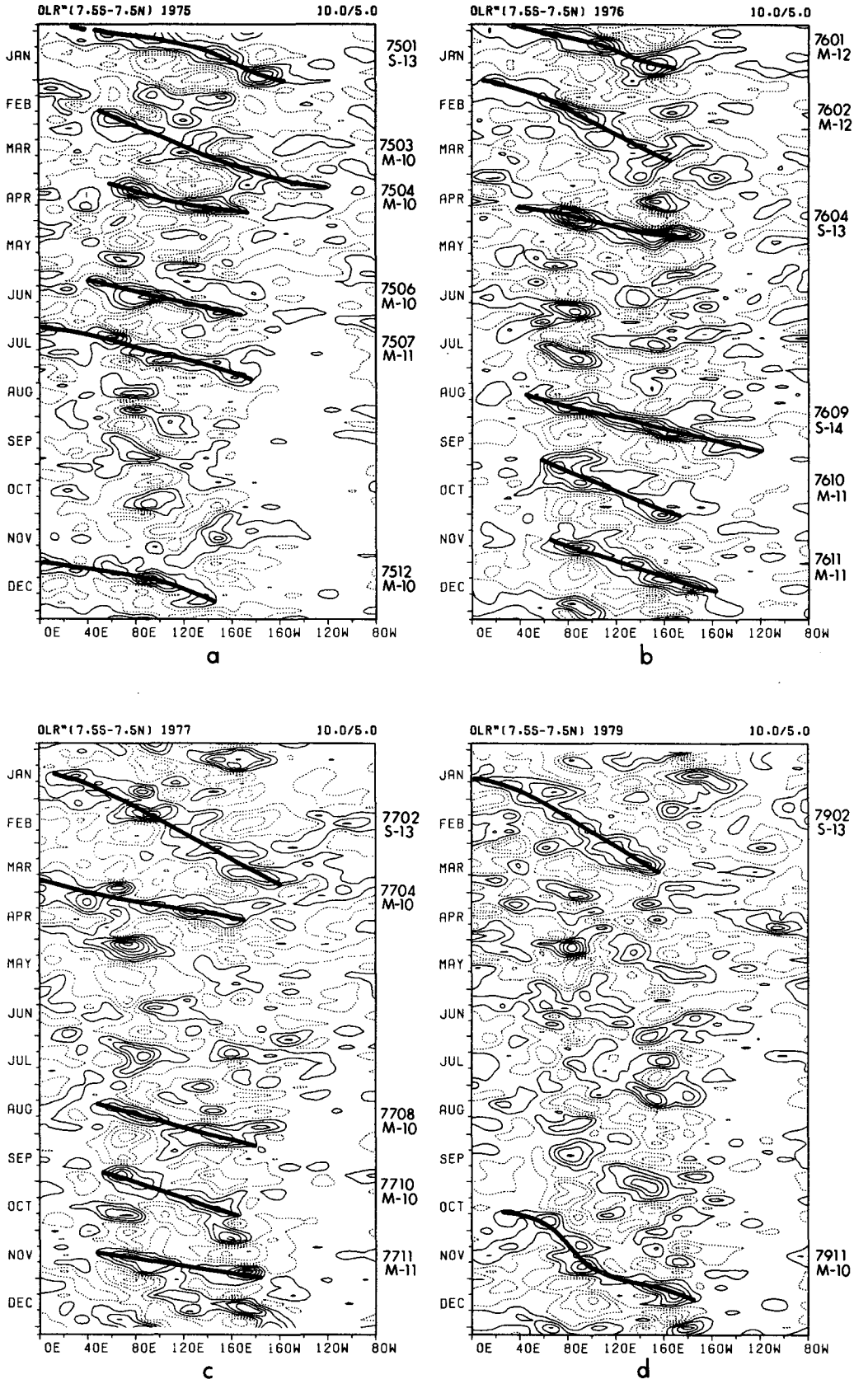

FIG. 1. Hovmöller diagram of pentad mean OLR anomalies averaged between 7.5°S and 7.5°N along the equator from 0°E to 80°W for 1975–77 and 1979–85. Contour interval is 10 W m^{-2}. Solid (dashed) contours indicate negative (positive) values equal or less (greater) than -5 W m^{-2} (5 W m^{-2}). Thirty-six selected eastward propagation events are marked out by heavy solid lines. The side notes include a tag number

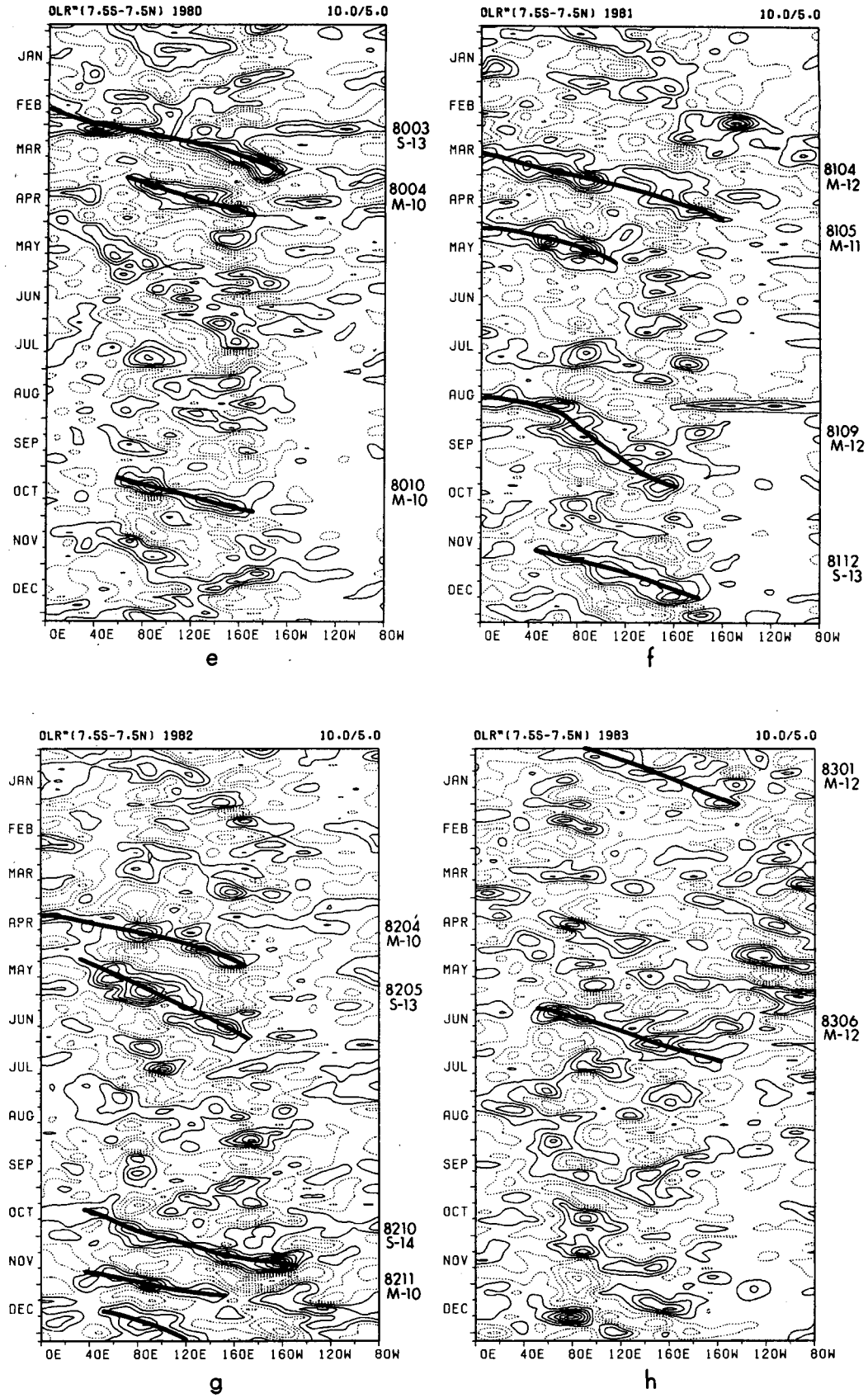

FIG. 1. (*Continued*) and classification (S—strong, M—moderate). The tag number denotes the year and month during which the most intense phase of the event occurs. The number following the classification letter is the intensity index defined in section 2.

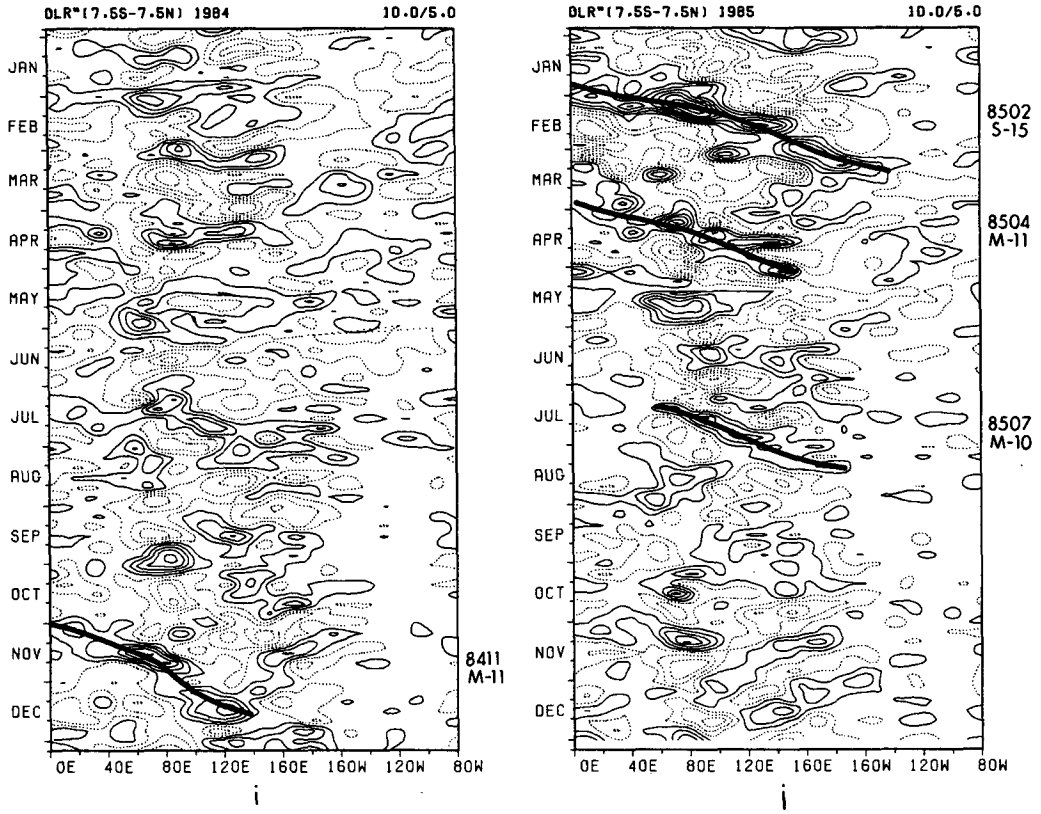

FIG. 1. (*Continued*)

(greater than 12), moderate (10–12) and weak (8–9). For the 10-year period, 65 events with more than 100° longitude of eastward displacement were selected; of these, 10 were strong events, 26 moderate and 29 weak. Each strong and moderate event is marked out by a heavy solid curve and a side note in Fig. 1.

c. *Composite procedure*

Previous studies determined composite phases based on a time series of zonal wind at fixed station (e.g., Madden 1986) or cyclic variation of the first two principal components (e.g., Knutson and Weickmann 1987; Murakami 1987). We determine the composite phases according to geographic locations of the anomaly centers. The dates when anomalous convection centers approximately pass through 30°E, 60°E, 90°E, 120°E, 150°E, 180°E, and 150°W were referred to as phases 1–7, respectively. Some events do not have all phases. For example, among 36 strong and moderate events, 6 terminated near 150°E. The composite at 180°E is then constructed by adding the other 30 cases but still dividing by 36. In this way, the composite intensities at different phases are comparable. Because of the composite method, the consolidated features described by composite maps are attributed to eastward propagating events with an average phase speed.

TABLE 1. Conversion of parameter values to scores.

Score	1	2	3	4
Total longitudinal displacement (longitude)	110–130	140–160	170–190	>200
Minimum OR″ contour value (W m^{-2})	−15	−25	−35	<−45
Mean duration (pentad)	1	2	3	4
Length of the gap (longitude)	25–30	15–20	5–10	0

3. Development characteristics

The composite OLR maps for 36 strong and moderate cases are presented in Figs. 2a–f. Since most events terminate near 180°, only 6 phases were constructed. At phase 1, a negative anomaly is centered over equatorial Africa (0°, 30°E), while there are positive (dry) anomalies located over the western Indian and western Pacific oceans, respectively. By phase 2, the negative anomaly over Africa propagates eastward to the western Indian Ocean (0°, 60°E), with significant intensification. The positive anomaly over the equatorial western Pacific shrinks considerably. At phase 3, the convection anomaly exhibits largest amplitude with OLR anomaly less than −27.5 W m^{-2} over the eastern Indian Ocean (0°, 90°E) in contrast with the positive (dry)

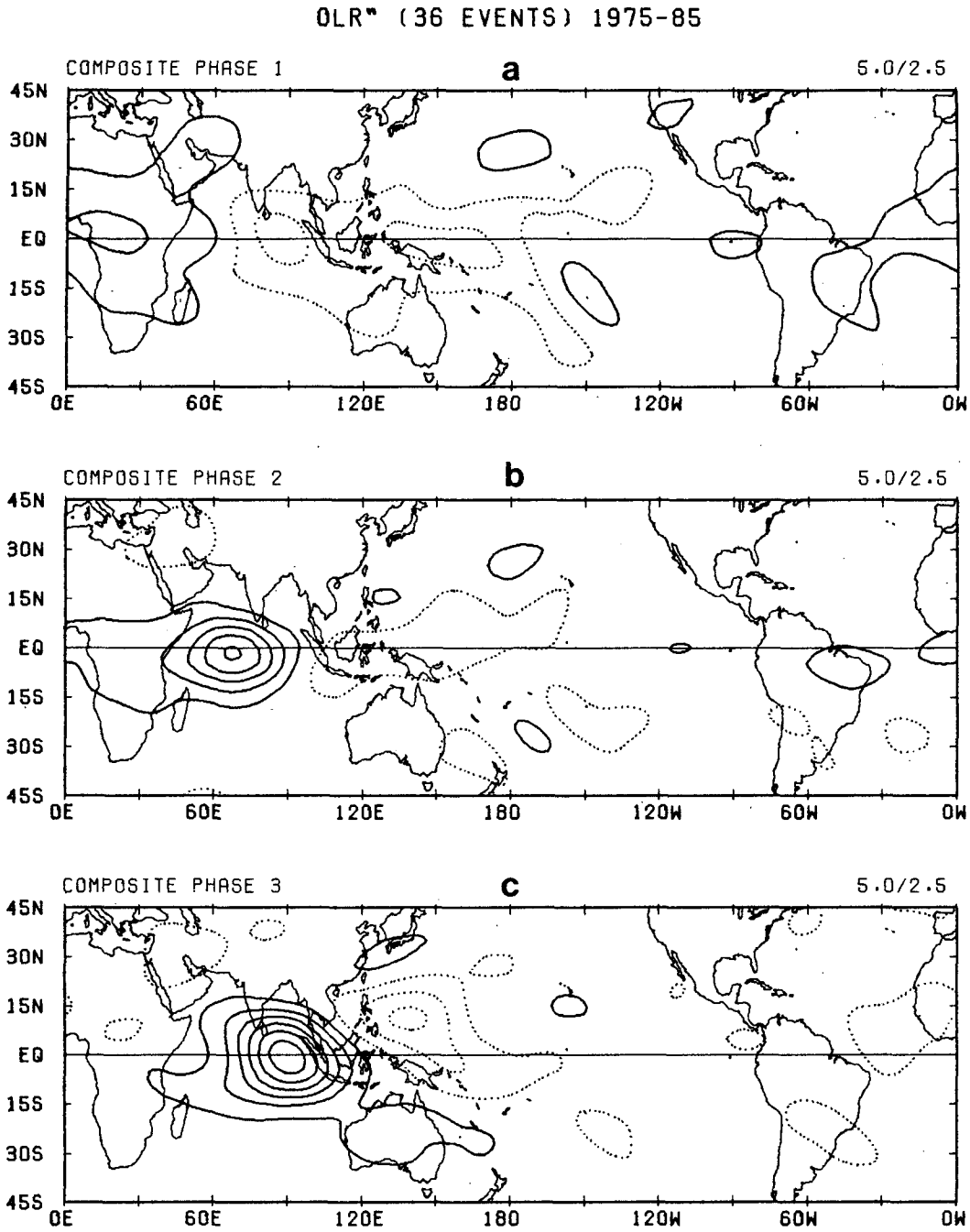

FIG. 2. Composite intraseasonal OLR anomaly charts of thirty-six events for phase 1 to phase 6. Contour interval is 5 W m^{-2}. Solid (dotted) contours indicate negative (positive) values equal or less (greater) than -2.5 W m^{-2} (2.5 W m^{-2}).

anomaly over the western North Pacific (10°N, 150°E). By phase 4, the negative anomaly over the eastern Indian Ocean reaches the maritime continent (0°, 120°E) expanding in area and weakening in strength. The dry area to the east has diluted.

An interesting feature is that from phase 1 to phase 3, the major positive anomaly center over the maritime continent–western Pacific stalls while the convection anomaly steadily migrates from equatorial Africa to the eastern Indian Ocean with rapid amplification. Consequently, the zonal gradient of OLR anomaly (hence, precipitational heating) dramatically increases over the maritime continent. This is followed by convection passing through the maritime continent, where

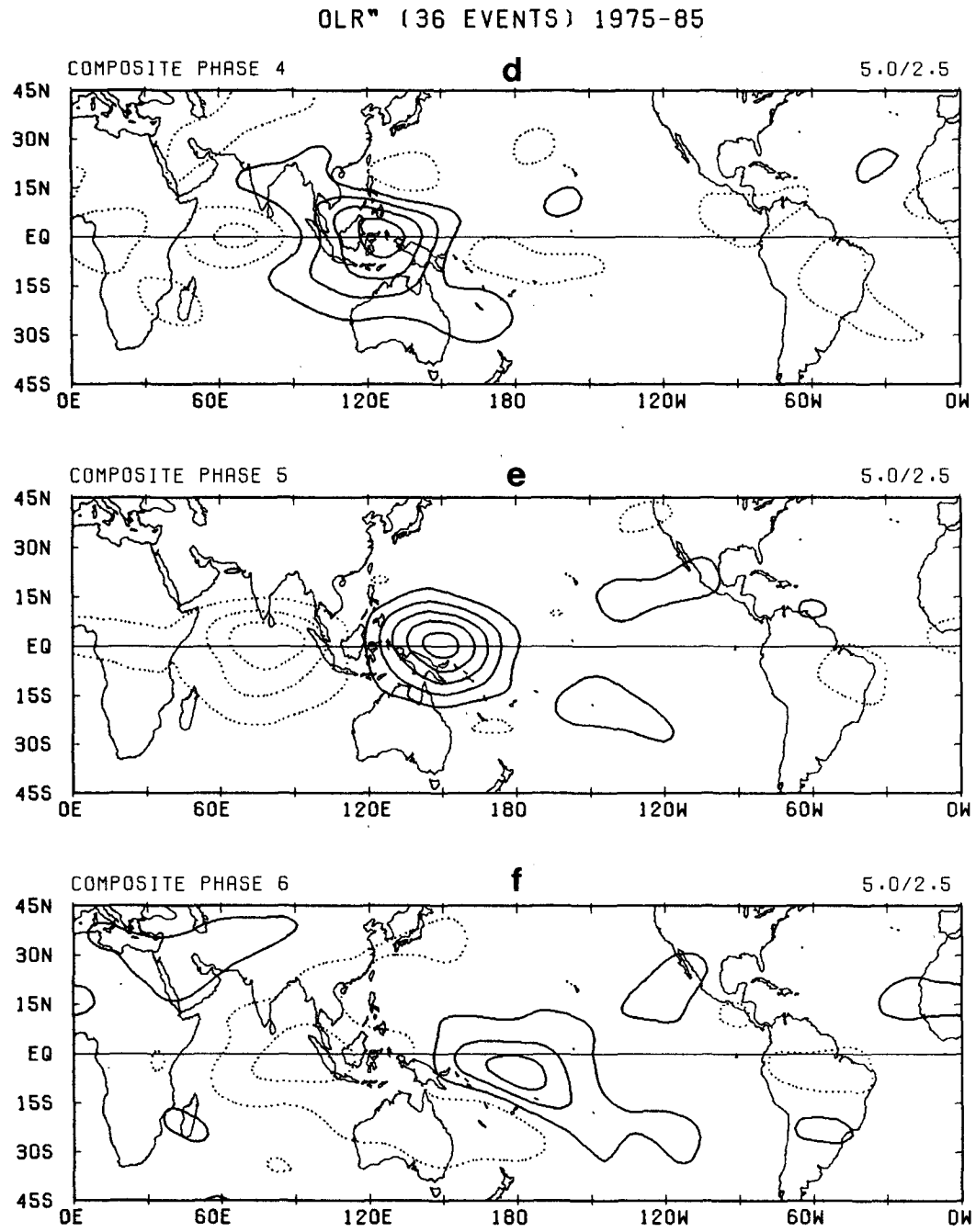

FIG. 2. (*Continued*)

a constant ascending branch of the Walker circulation persists. Meanwhile, the originally near-stationary dry region over the western Pacific is pushed further east with remarkable weakening. A new dry region starts to form over Africa–the western Indian Ocean.

The negative anomaly propagates eastward to the equatorial western Pacific (0°, 150°E) from phase 4 to phase 5, and correspondingly, the dry center moves from the western to eastern Indian Ocean, reaching a maximum anomaly of 17.5 W m^{-2} by phase 5. At this stage, the anomalous convection is slightly reenhanced over the western Pacific. From phase 5 to phase 6, the negative anomaly weakens and moves further east to the date line. A positive anomaly covers the entire Indian Ocean, maritime continent, and northern Australia.

Main features of the composite OLR anomalies shown in Fig. 2 are summarized as follows. Organized large scale OLR anomalies generally form over equatorial Africa and systematically move eastward to the equatorial central Pacific after their inception. Clear evidence of rapid developments, which usually takes place over the Indian Ocean, suggests that the eastward propagating modes are unstable. The composite rate of intensification for the OLR low is about 15 W m^{-2} per pentad. An individual event usually has a greater deepening rate of 25 W m^{-2} per pentad. Mean propagation speed is about 4°–6° longitude per day. The fastest propagation is from phase 5 to phase 6 (about 6° longitude day^{-1}) and the slowest movement is from phase 2 to phase 3 (less than 4° longitude day^{-1}). This appears to suggest that the phase propagation tends to slow down during intensification and speed up during weakening. The average life span is about 42 days. The strongest negative anomalous OLR (−27.5 W m^{-2}) occurs over the eastern Indian Ocean at phase 3, and the strongest positive anomaly (17.5 W m^{-2}) also occurs in the Indian Ocean but at phase 5.

Composite OLR anomaly maps at different phases for 26 moderate and 10 strong cases were also constructed separately (not shown). The main features of both composites are similar to the composite of 36 cases from phase 1 to phase 6. Several noteworthy differences exist, however, between strong and moderate composites. First, in the moderate-case composite, the intensity of convection remains the same when it moves from the maritime continent to western Pacific; the convection dissipate rapidly from the western Pacific to the date line. In the strong-case composite, however, the convection significantly reintensifies over the western Pacific after passing through the maritime continent and there is little decay from the western Pacific to the date line. Significant weakening occurs when the convection center moves to 150°W. Thus, strong events have longer life spans and greater longitudinal displacements due to the reenhancement of convection in the western Pacific. Second, when strong OLR anomalies reach the equatorial central Pacific, the negative OLR anomalies tend to emanate away from the equator toward North America and southeastern Pacific, suggesting the existence of intraseasonal tropical–extratropical interaction. On the other hand, for the moderate-case composite these tendencies are rather weak.

4. Composite horizontal structure

Six strong events that occurred between 1979 and 1985 were used to construct composite structure due to the limited period of availability of ECMWF wind data. Another reason for choosing only strong cases is that the wind fields associated with strong convective activity are expected to have pronounced signals. Therefore, the composite dynamic structure of strong events should definitely be more detectable and statistically significant. Of the six strong events, four occur during December to March and the other two during transition periods (May and October) of 1982. These composites basically represent boreal winter. The fact that most strong events occur in boreal winter supports the notion that intraseasonal oscillation in the equatorial region exhibits significant annual variation. This agrees with Madden's (1986) finding.

a. Convection and vertical motion anomalies

Maps of OLR anomaly composite for six strong cases are presented in Fig. 3. Comparing Fig. 3 with Fig. 2, one can readily find that the main features of both composites from phase 1 to phase 6 are similar, but the six-case composite contains some detailed information and, in general, both the negative and positive anomalies are larger. Since the convection anomalies in most strong events reach 150°W, phase 7 was added for the six-case composite. It is noteworthy that when strong convection anomalies move eastward crossing the maritime continent (Fig. 3d) there exist two OLR troughs extending from Borneo to the Arabian Sea and central southern Indian Ocean, respectively. These tilted OLR troughs when moving eastward yield poleward components of the movement in the monsoon regions. Using a high resolution dataset, Krishnamurti et al. (1985) illustrated a tilted system in the velocity potential field that moves northeastward in the Indian monsoon region and eventually eastward away from the monsoon region. The features seen from OLR composites seem to be consistent with their analysis of the evolution of velocity potential field.

In order to explore the primary structure of the low-frequency motion, the wind divergence at 200 mb and 850 mb were calculated. The difference of divergences between 200 mb and 850 mb was then computed. The differential divergence, $D_{200}-D_{850}$, can be considered as an estimate of the vertical motion at middle troposphere.

In Fig. 4, the differential divergence anomalies for composite phases 1–7 are presented. A rising motion area over tropical Africa in phase 1 overlaps negative OLR anomalies. By phase 2, it rapidly shifts to eastern central Indian Ocean, meanwhile a sinking motion area develops over the maritime continent–northern Australia. From phase 2 to phase 3, both the rising motion and the sinking motion regions intensify. At phase 4 the large differential divergence anomaly moves into the maritime continent and reaches its maximum magnitude of order (10^{-6} s^{-1}). From phase 4 to phase 7, the ascent area moves steadily eastward to the central Pacific, maintaining its intensity. The subsidence region over the eastern Indian Ocean expands and finally covers the entire maritime continent.

Because values of divergence at 200 mb are much larger than those at 850 mb, spatial patterns of vertical

motion are similar to those of 200 mb divergence; however, 850 mb wind divergence also contributes to the vertical motion field. Therefore, the coherence between vertical motion and equatorial convection is more significant. In Fig. 4, rising motion regions are always nearly coincident with negative OLR anomalies. The eastward movement for rising motions is quite clear; that of sinking motion is less so. This implies that the low-frequency motion is asymmetric with respect to time (wet and dry phase). It may be considered more as an event-like phenomenon rather than cyclic or oscillatory.

b. Composite wind anomalies at 200 mb

Composite maps of 200 mb wind anomalies for the six strong cases are shown in Fig. 5. Let us first focus on the wind field in the equatorial zone between 15°S and 15°N. A pronounced feature is that a large-scale easterly anomaly region propagates eastward from the Atlantic and equatorial Africa to the central Pacific, roughly in correspondence with the eastward movement of the negative OLR anomaly. Less evident is the tendency of upper-level equatorial westerly anomaly to accompany a positive OLR anomaly, shifting eastward. The eastward propagating 200 mb zonal wind anomaly is of global extent (both wave 0 and wave 1 make strong contributions), which is larger than the corresponding length scale of OLR anomaly. This is consistent with the results of Liebmann (1987).

The equatorial zonal wind anomalies are closely associated with subtropical wind systems. At phase 1 (Fig. 5a), two anticyclonic cells located over the North Africa (7°N, 40°E) and south African coast are linked to the equatorial easterlies. From phase 1 to phase 2, the equatorial easterlies extend to the Indian Ocean with significant intensification. To the north of the equatorial easterlies the anticyclone develops in the northern Arabian Sea with a east–west ridge stretching from north Africa to southeast Asia. The Southern Hemisphere anticyclonic cell also extends eastward from southern Africa to the southern Indian Ocean. By phase 3, the easterlies uniformly cover a broad tropical region from about 25°S to 20°N with little eastward movement. Since the convection has moved from the western to eastern Indian Ocean, the strongest easterlies lag the convective center by about 40° longitude.

The strong anomalous easterlies move to the Northern Hemisphere tropics by phase 4. The elongated anticyclonic systems in both subtropics also shift eastward. From phase 4 to phase 5, the easterly anomalies move southeastward from south Asia to the eastern maritime continent. The subtropical anticyclonic systems tend to move ahead of the equatorial convective center.

In phases 6 and 7, the convection quickly moves eastward to 180° and weakens afterwards (Figs. 3f, g). The zonal component of the wind field near the convective center weakens correspondingly. The anticyclonic cells in both hemispheres tend to merge over the central–eastern Pacific with meridional flow across the convective center from the Southern to Northern Hemispheres. The cross-equatorial flows near the date line are divergent winds consistent with the strong ascent center in the Southern Hemisphere at 15°S, 165°W and descent area in the Northern Hemisphere at 20°N, 170°W (Fig. 4f).

One may also find that after the mature stage (phases 3–7), significant westerly anomalies occurring to the east of the convective region are between two subtropical cyclonic centers located at 15°S and 15°N, respectively (Figs. 5c–g). Therefore, the overall anomaly pattern consists of equatorial easterlies overlapping the convection and westerlies east of the convection, with easterlies coupling with twin anticyclones and westerlies coupling with twin cyclones on both subtropics. To some extent, this pattern is similar to Gill's stationary circulation driven by a symmetric equatorial heat source, but there are two important differences. First, Gill's pattern does not have twin cyclones coupling with westerlies to the east of the heating. Second, in Gill's solution, the westerlies east of the heating center have a longitudinal extent nearly three times that of easterly anomalies to the west of the heating center, while the extent of westerly anomalies in the present composite is smaller than that of the easterly anomalies. A similar difference was noticed by Rosenlof et al. (1986) in comparing their model-simulated Walker circulation and Gill's steady state solution. Nevertheless, the similarity between horizontal structure of composite convection–wind anomalies and Gill's solution suggests that the low-frequency equatorial mode is not a pure moist Kelvin mode but involves a coupling of equatorial Kelvin and Rossby waves.

c. Composite 850 mb wind anomalies

Figure 6 presents composite 850 mb anomalous wind fields for the 6 strong cases. At phase 1, there are two weak cyclonic circulation cells, one over the Middle East (30°N, 30°E), and the other over South Africa. The westerlies between these two cyclones are coupled with the convection over equatorial Africa. From phase 1 to phase 2, the Northern Hemisphere cyclone moves southeastward to 18°N and 50°E, and the Southern Hemisphere cyclone shifts eastward to the African coast. Simultaneously, the westerlies between these cyclones extend to the equatorial Indian Ocean and intensify. A noticeable feature in Fig. 6b is the northerly flow penetrating from southern Europe across northern Africa to the equator. This flow can significantly enhance downstream westerlies.

In phase 3, the Northern Hemisphere cyclone moves further east to the western Indian coast (15°N, 70°E), with a trough to the southwest, and the Southern Hemisphere cyclonic cell moves eastward and inten-

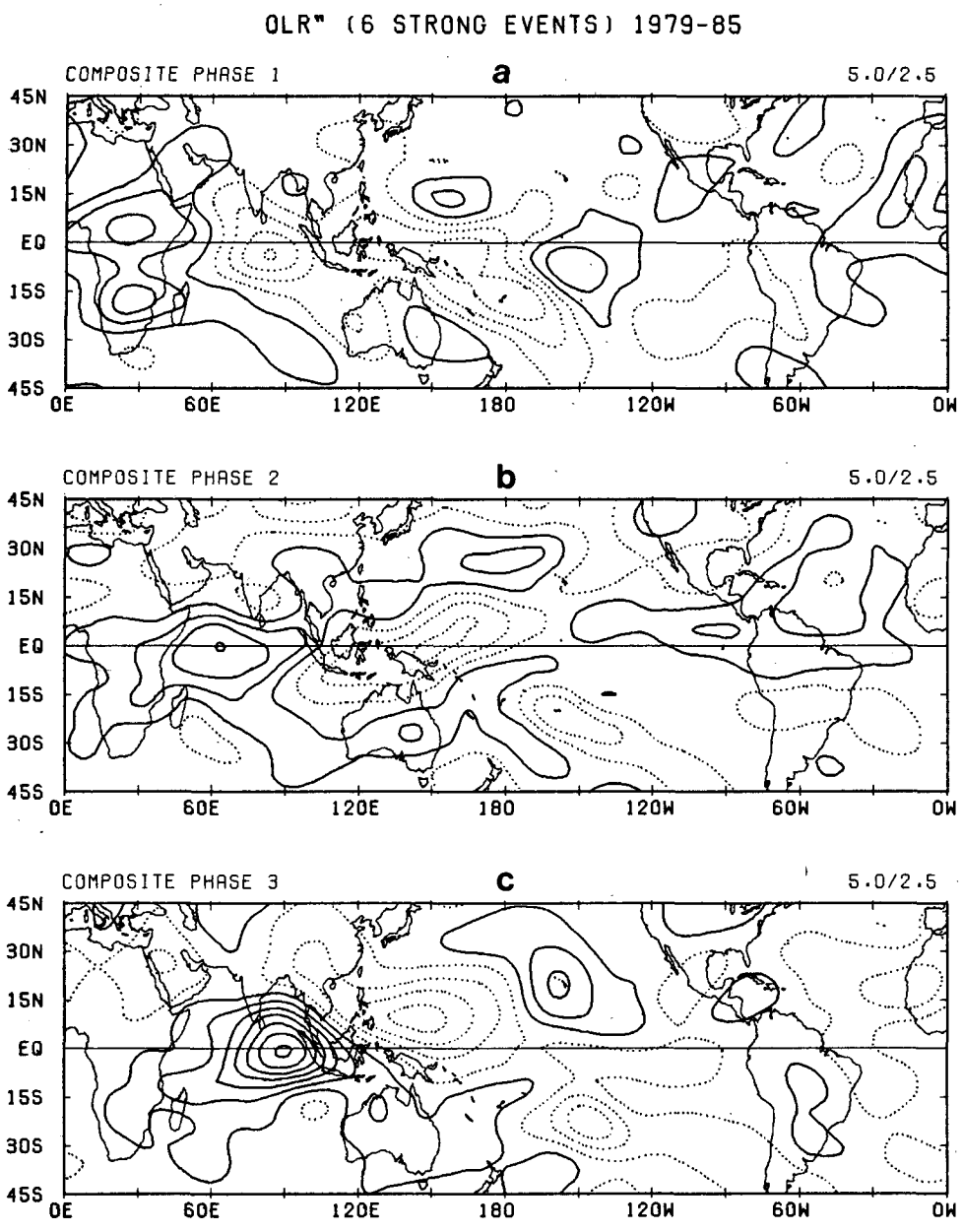

FIG. 3. As in Fig. 2, but for seven phases of six strong events that occurred during 1979–85.

sifies with a trough oriented northeast–southwest across the Indian Ocean. By phase 4, the equatorial westerlies extend to the maritime continent and are associated with a Northern Hemisphere trough (shear line) extending from east of Japan to the Arabian Sea and a Southern Hemisphere trough from the southern Indian Ocean to northern Australia. These systems are so well organized that the embedded equatorial westerlies cover the entire Indian Ocean with a maximum west of convection center. From phase 4 to phase 6, the equatorial westerlies and associated twin cyclonic systems propagate from west of the maritime continent to the date line and weaken afterwards without appreciable movement.

It is interesting to note that at 850 mb the equatorial easterlies generally accompany but trail slightly the dry regions and tend to couple with twin anticyclones or anticyclonic ridges residing each hemisphere's subtropics. The easterly anomalies are comparable with the westerly anomalies in both strength and longitudinal extent.

d. Relation to previous work

From Figs. 5 and 6, it is evident that at both 200 mb and 850 mb, two types of coupling exist. One is the coupling between equatorial easterly (westerly) anomalies and subtropical anticyclonic (cyclonic) cir-

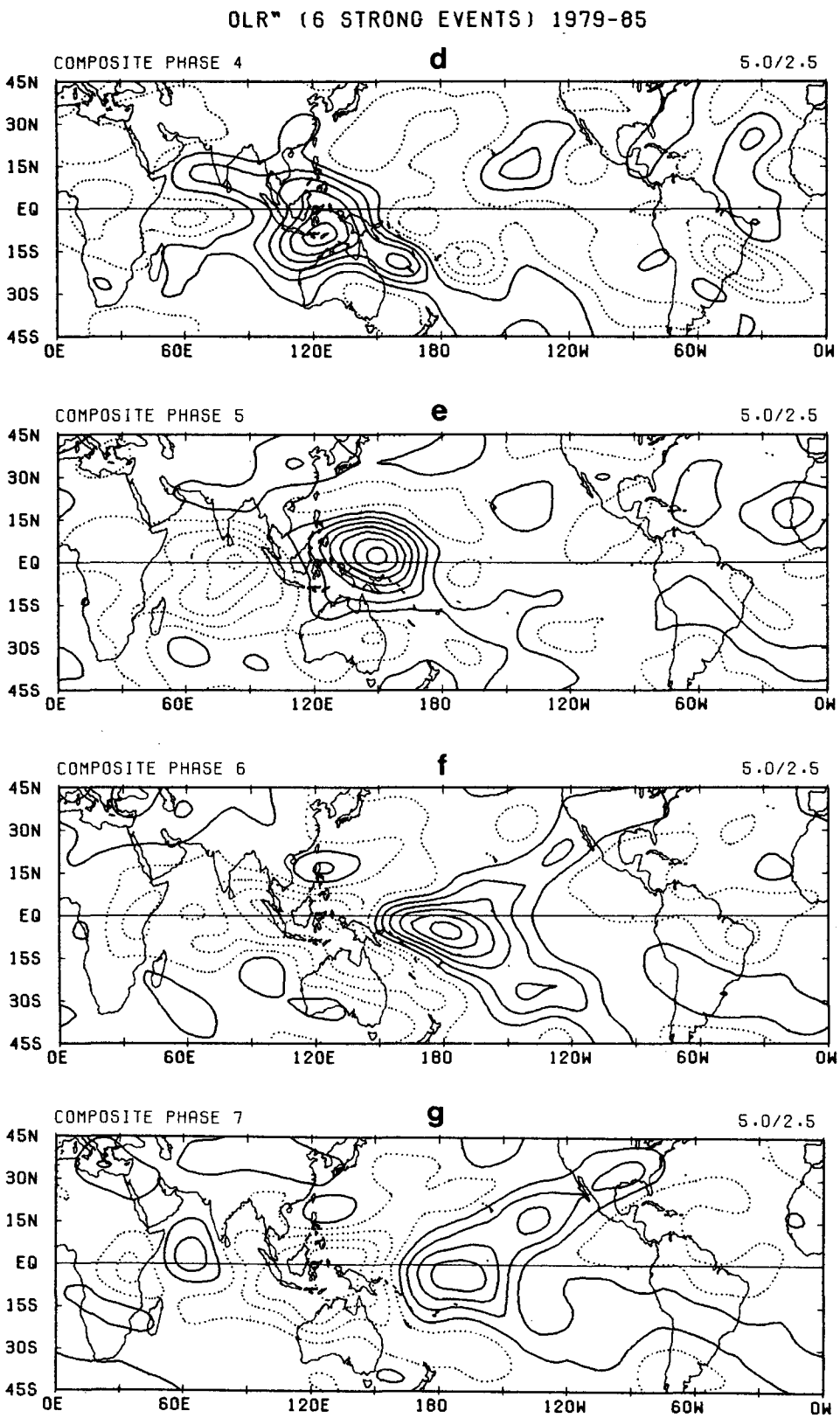

FIG. 3. (*Continued*)

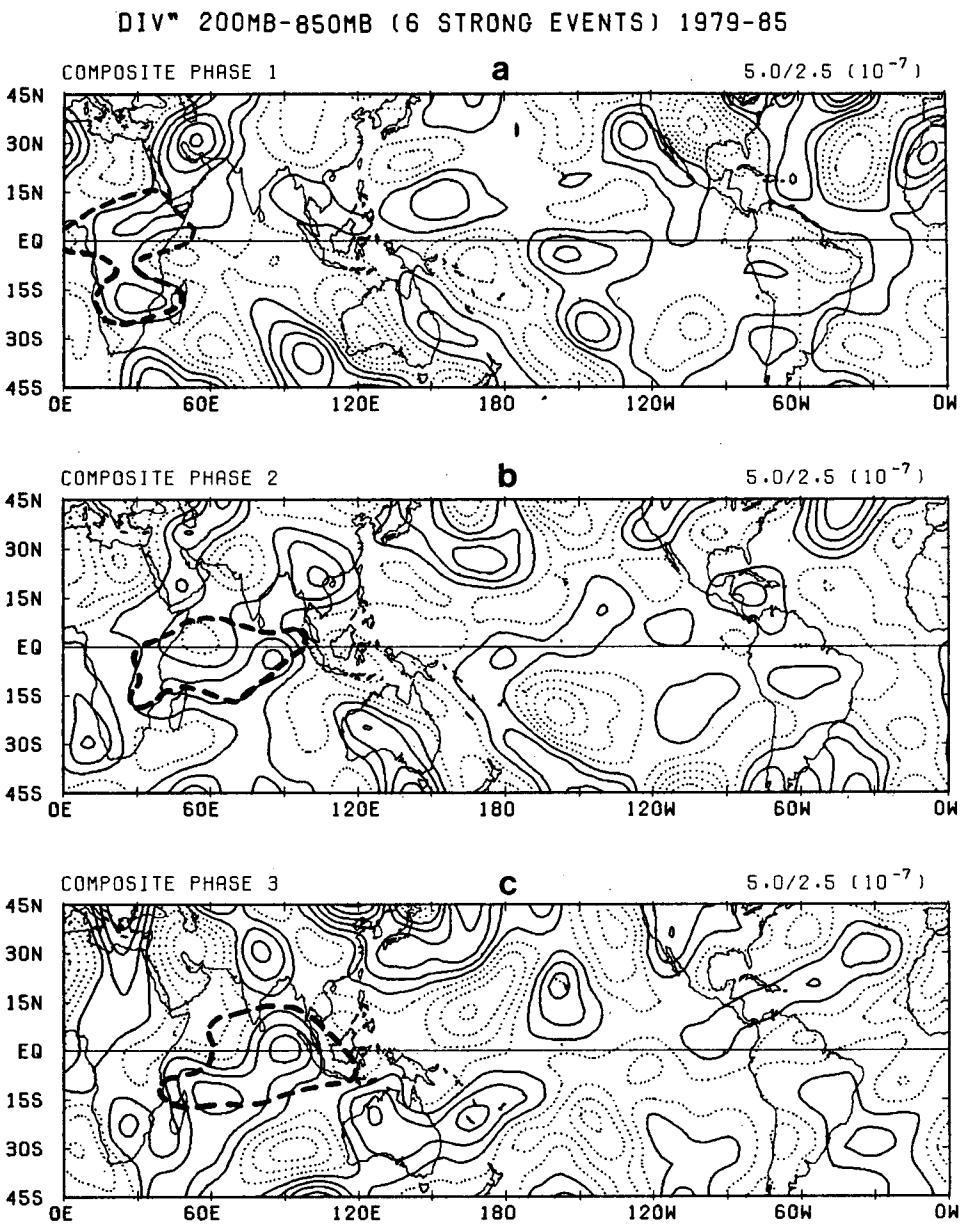

FIG. 4. Composite charts of divergence difference between 200 mb and 850 mb, (D_{200}–D_{850}), for six strong events from phase 1 to phase 7. Contour interval is 5.0×10^{-7} s^{-1}. The solid (dashed) contours denote positive (negative) values equal or greater (less) than 2.5×10^{-7} s^{-1} (-2.5×10^{-7} s^{-1}). Also shown are the OLR contours of -7.5 W m^{-2} at corresponding phases (thick dashed curve).

culations of both hemispheres. They form a consolidated wind system which maintains the equatorial upper-level easterlies and low-level westerlies at each composite phase. The other is the coupling between the circulation anomalies and tropical convection. These couplings provide a coherent structure in accord with the development and eastward propagation of the low-frequency motion.

Madden (1986) and Knutson and Weickmann (1987) examined the relationship between OLR anomalies and upper-tropospheric (150 mb or 250 mb) wind anomalies in solstice seasons. Madden found only anticyclones even with and to the west of regions of convective forcing, while Knutson and Weickmann noticed cyclones east of the anomalous convection as well. Both of them emphasized asymmetric response in solstice seasons but with opposite conclusions: Madden's picture has a dominant anticyclone in the summer hemisphere, whereas Knutson and Weickmann's exhibits pronounced rotational wind anomalies in the winter hemisphere. The sequence of circulation anomalies at 200 mb (Fig. 5) at phases 3 and 5 bears

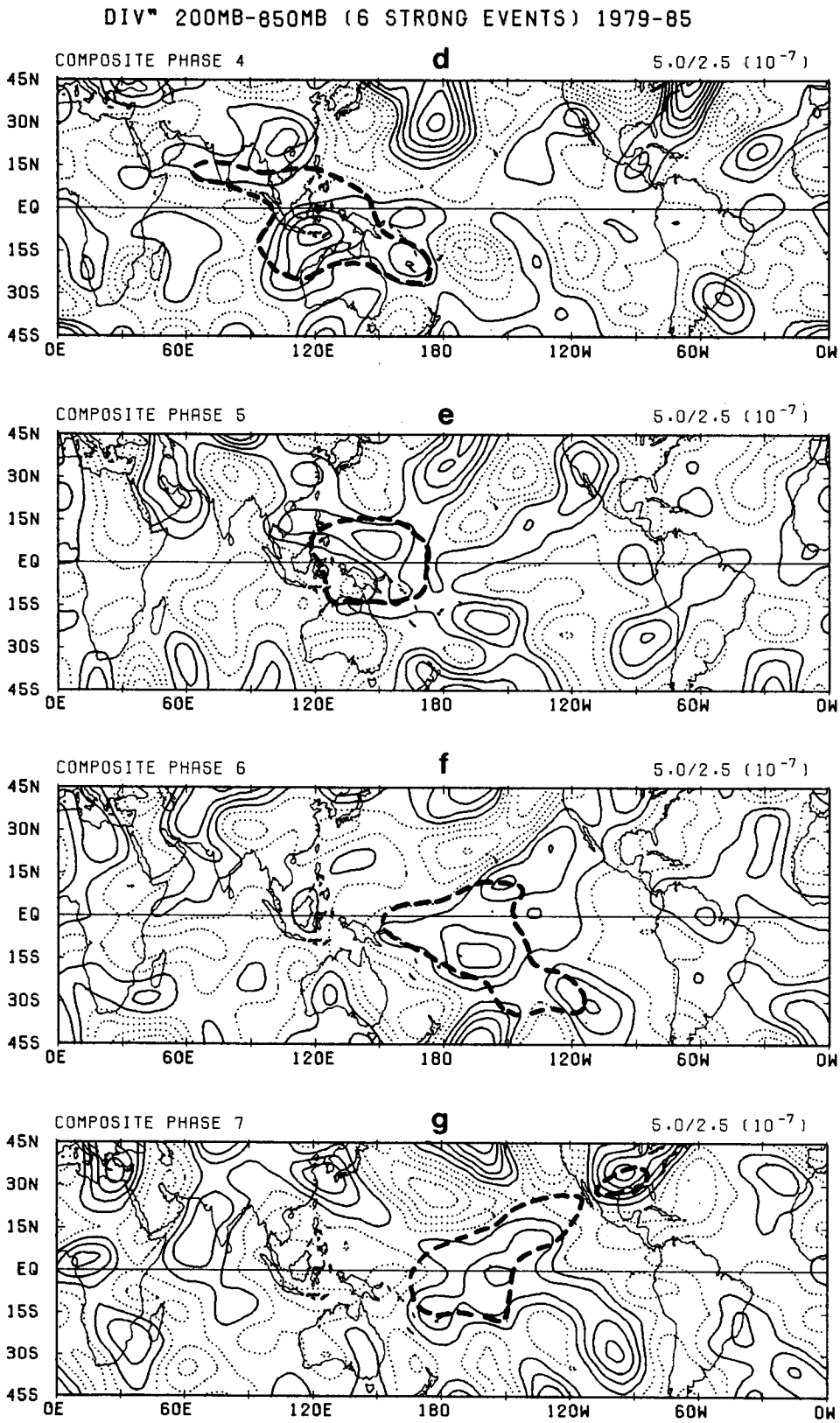

FIG. 4. (*Continued*)

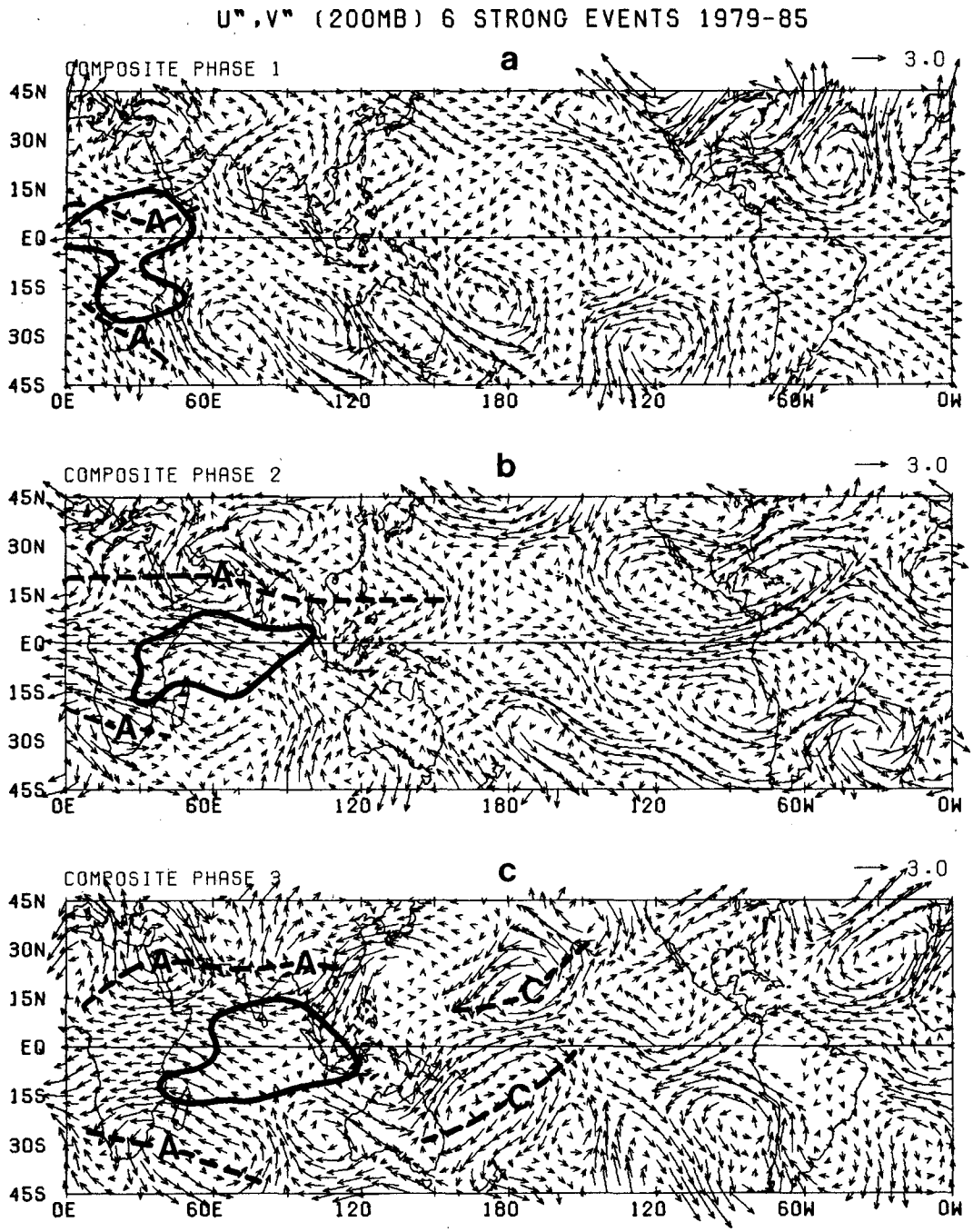

FIG. 5. Composite 200 mb anomalous wind charts of the six strong events for phases 1–7 (expressed in m s^{-1}). Also shown are the OLR anomaly contours of −7.5 W m^{-2} at corresponding phases (thick solid curves), major ridges or troughs (thick dashed lines), and major anticyclonic (A) and cyclonic (C) centers.

resemblance to Knutson and Weickmann's description. Our patterns, however, show a dominant symmetry of cyclonic and anticyclonic circulation about the equator. The qualitative features from phase 3 to phase 5 in Fig. 5 are also similar to the composite patterns for northern winter rotational components observed by Murakami (1988). The circulation patterns at phases 1, 2, 6, and 7 are not comparable with previous studies due to different compositing procedures. The 850 mb circulation anomalies at phases 3–5 are to a large extent consistent with Murakami's (1988), but noticeable differences exist. One difference is the strength of the zonal wind anomalies and the coupled patterns. When the convection anomalies are over the Indian and western

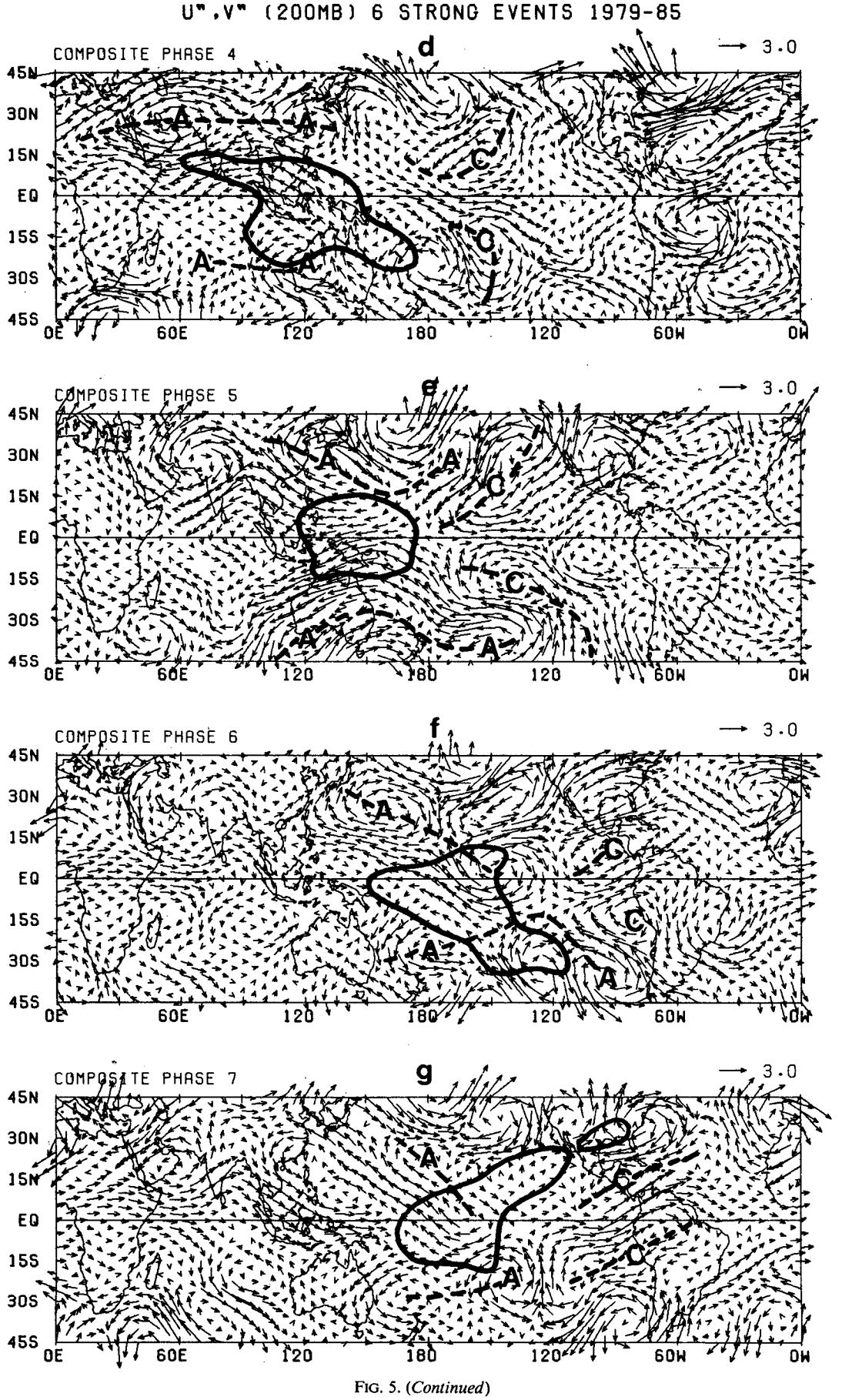

FIG. 5. (*Continued*)

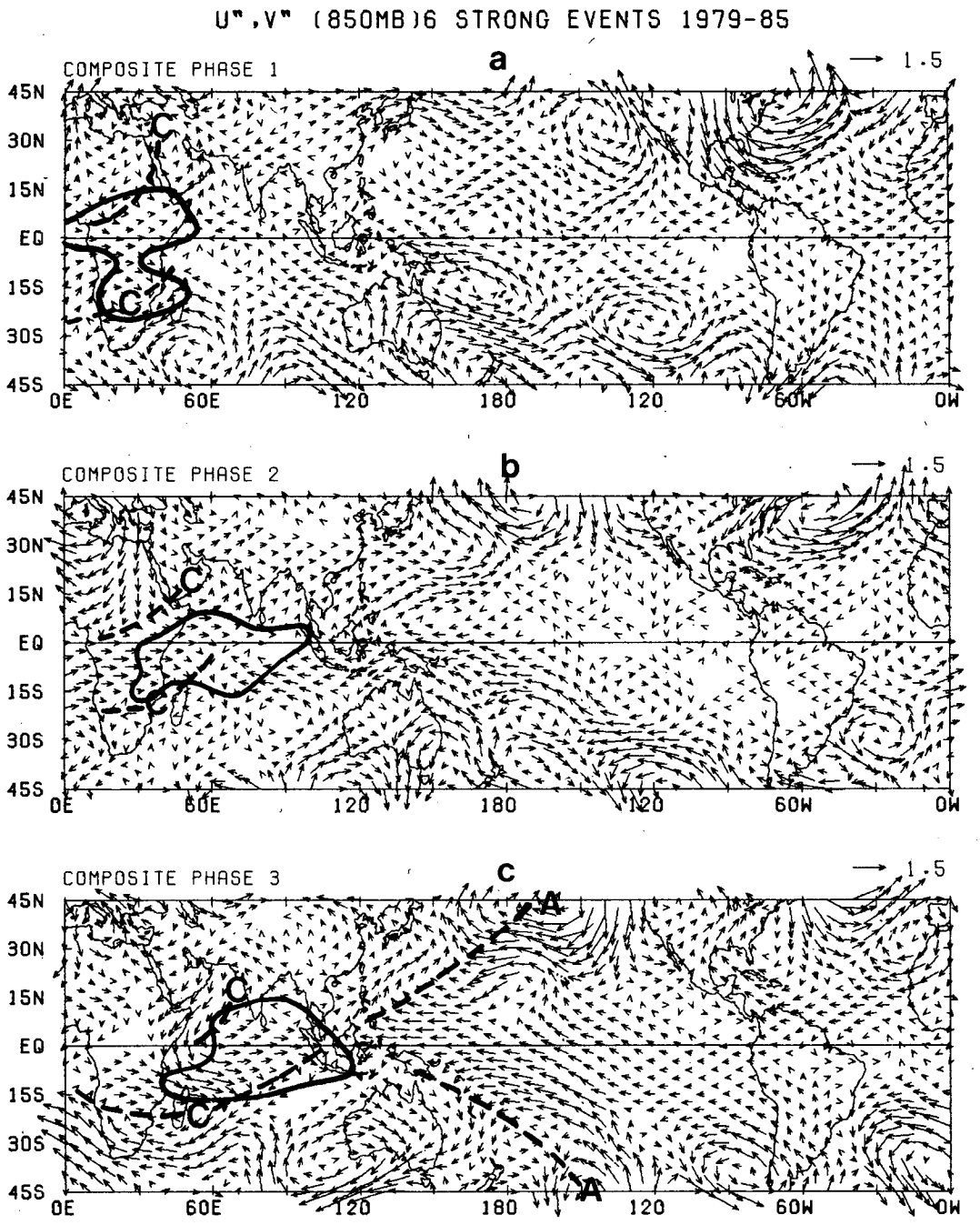

FIG. 6. As in Fig. 5, but for 850 mb wind anomalies.

Pacific oceans, our results show much stronger zonal wind anomalies and better organized cyclonic and anticyclonic systems coupled with the equatorial zonal wind anomalies. This is probably due to the fact that we only chose strong events. In addition, our composite shows that the 850 mb circulation anomalies tend to be confined within the eastern hemisphere in harmony with the evolution of the OLR anomalies, while the 200 mb circulation anomalies can travel across the eastern Pacific. This point will be further elaborated in section 6.

5. Vertical structure in the equatorial zonal plane

The OLR, zonal wind and divergence anomalies at 200 mb and 850 mb as well as the midtropospheric vertical velocity in the equatorial belt between 7.5°N and 7.5°S are presented in Fig. 7. The intraseasonal

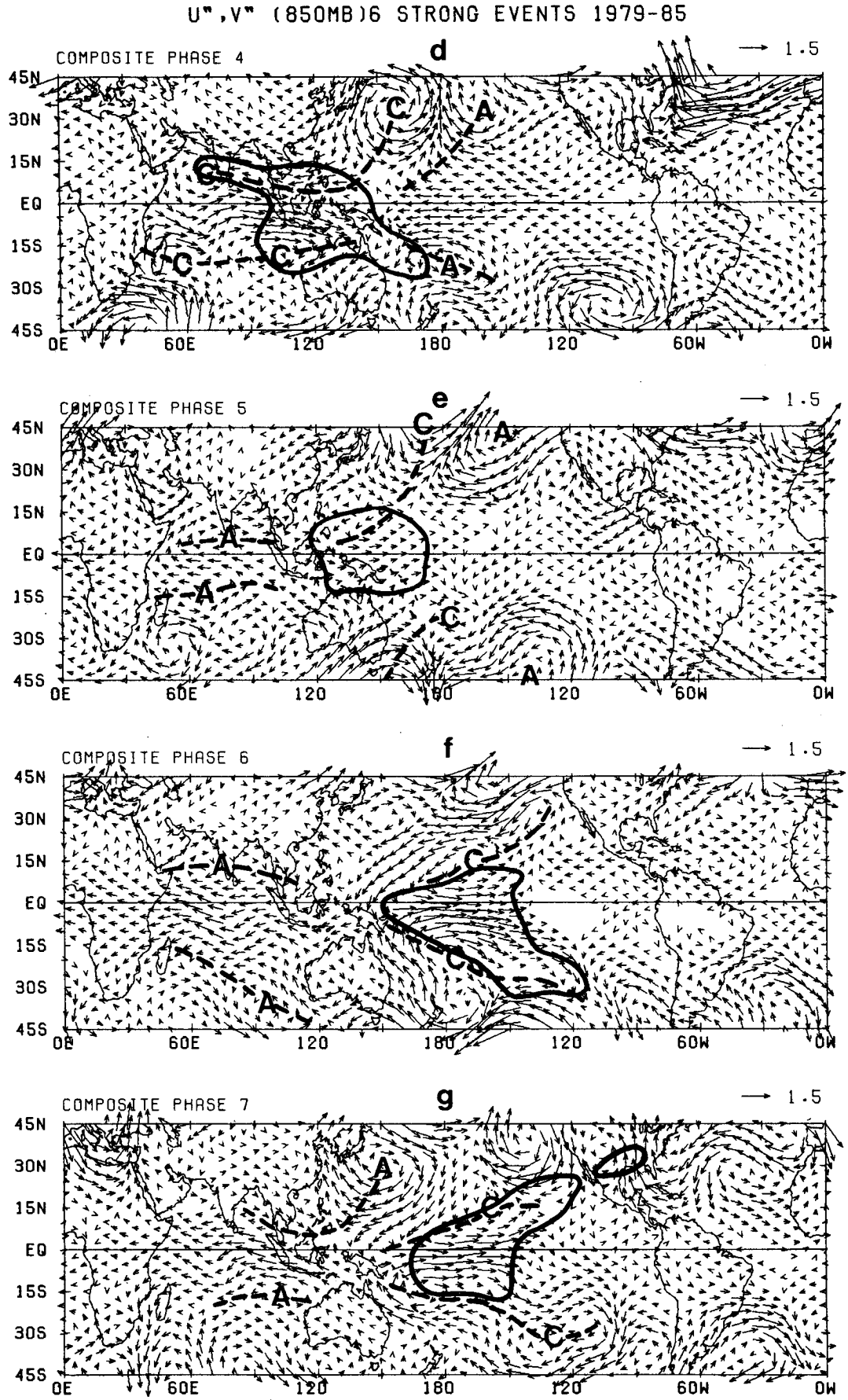

FIG. 6. (*Continued*)

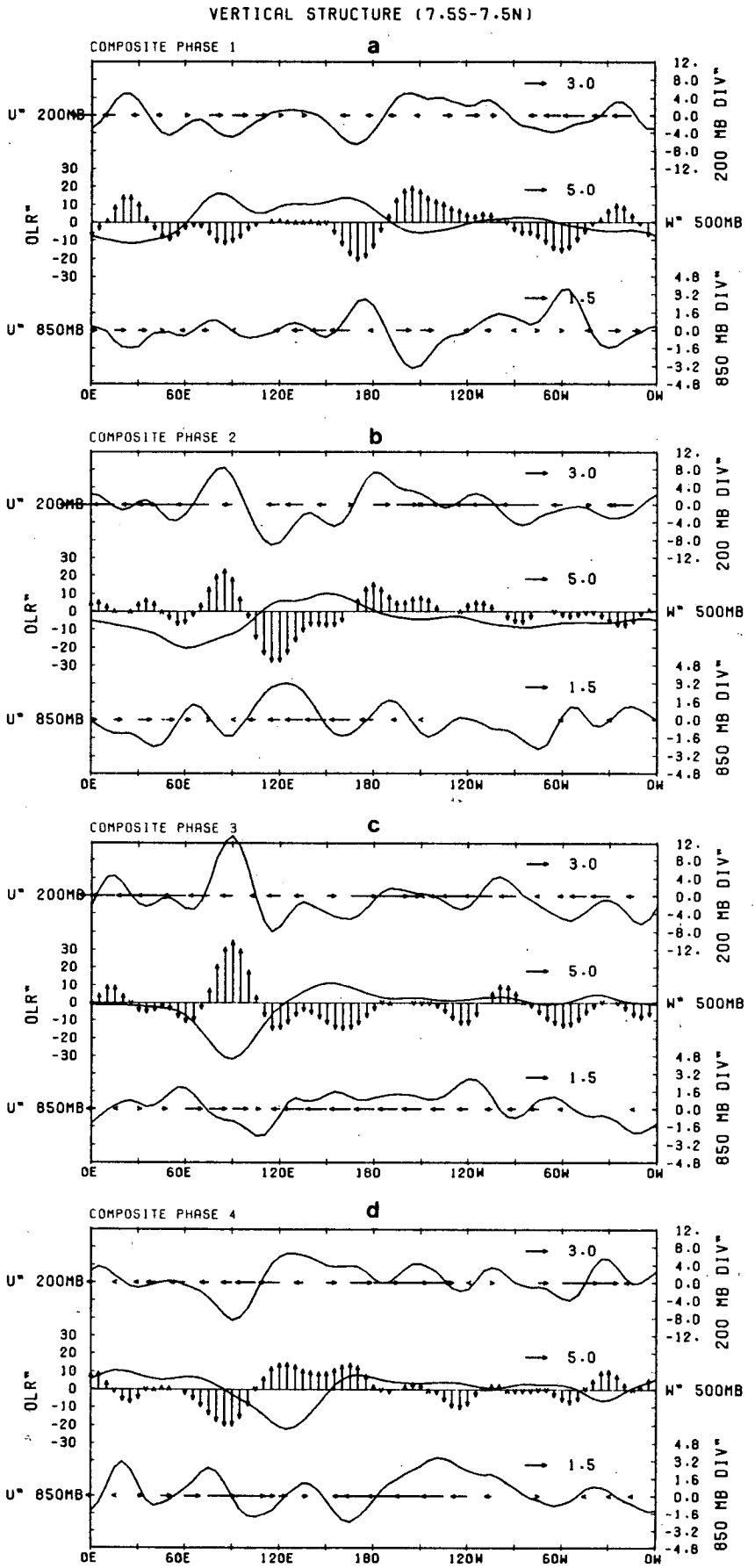

FIG. 7. Vertical structure in the equatorial zonal plane of composite anomalous OLR, 200 and

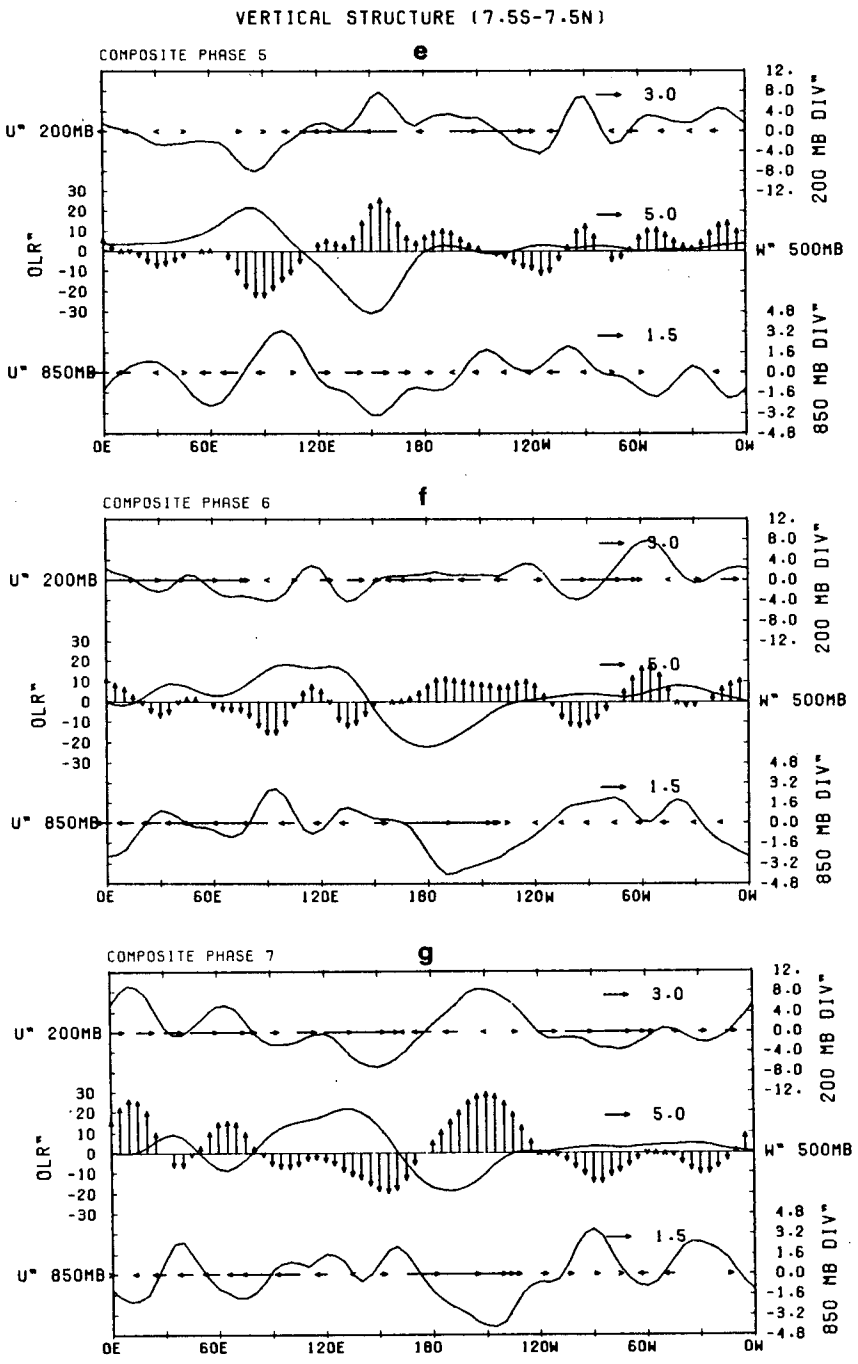

FIG. 7. (*Continued*) 850 mb zonal winds (U'') and divergences (DIV$''$), and the differential divergence (W'') for the six strong events from phase 1 to phase 7. The values are obtained by latitudinal average between 7.5°S and 7.5°N. Units are W m^{-2} for OLR, m s^{-1} for zonal wind U'', 10^{-7} s^{-1} for divergence DIV$''$ and differential divergence W''.

low-frequency anomalies in the equatorial belt have a primary length scale of zonal wavenumber 2 for OLR and nearly wavenumber 1 for zonal wind. Yet, a well-defined relationship between convection and zonal winds is readily seen in the neighborhood of the strong convection, where the low-frequency motion has large amplitude. From phase 1 to phase 6, the equatorial convection and lower-level westerlies and upper-level easterlies move eastward together, but a difference in the phase speeds between the convection and zonal

winds exists. Therefore, the phase relationships among OLR and zonal wind anomalies at 200 mb and 850 mb change with composite phases. Focusing on the longitude of pronounced amplitude of OLR west of the date line, one finds that, in phase 3, the easterly anomaly center at 200 mb is about 40° longitude behind the convection center. Because of faster propagation, the 200 mb easterly anomaly catches the convection anomaly at phase 5. By phase 6, the convection is centered at the date line, while the upper-level easterly center is 10° longitude ahead. The lower-level westerly center also moves faster than the convection, and it catches the convective center at phase 6. A similar result was observed by Knutson and Weickmann (1987). They found OLR fluctuations over the eastern hemisphere are phase locked to the global-scale velocity potential wave at 200 mb with the largest OLR anomalies exhibiting a slightly slower eastward progression, particularly during May–October. The present analysis indicates that during northern winter the phase speed difference between OLR and equatorial zonal wind anomalies is more evident than that between the OLR and divergence anomalies at 200 mb.

Another basic feature is that the zonal wind at 850 mb is nearly out of phase with that at 200 mb. This confirms conclusions derived from previous cross-spectral and EOF analyses (e.g., Madden and Julian 1972, and many others). In addition to the baroclinic structure of the zonal wind anomalies, we emphasize that the amplitudes of zonal wind fluctuation are unequal at the upper and lower levels; rather, the amplitude at 200 mb is about twice that at 850 mb. The asymmetric zonal wind fluctuation with respect to the midtroposphere, with the upper-level fluctuation dominating, suggests that the lowest baroclinic mode alone is insufficient to account for the characteristic vertical structure.

The anomalous OLR and divergences at both levels are highly correlated on the longitudes where the OLR anomalies are pronounced, although the zonal scale of divergence fluctuation at each level is smaller. When the negative OLR anomaly reaches a minimum at 90°E in phase 3, the 200 mb divergence reaches its maximum: 1.4×10^{-6} s^{-1}. The 200 mb divergence anomalies nearly top the strongest convection anomaly at most of the phases except phases 2 and 7, during which the upper divergence centers are about 20°–30° longitude ahead of the corresponding convection centers. On the other hand, the 850 mb convergence anomalies always tend to lead the convection after the inception of the OLR anomaly. Because the intensity of 200 mb divergence dominates in determining midtropospheric vertical motion, the anomalous rising motion is nearly in phase with 200 mb divergence and convection anomalies.

Close association between positive OLR anomaly and upper-level convergence can also be found in Fig. 7. For phases 2, 3, and 5, the upper-level convergence is consistent with positive OLR anomalies centered at 120°E, 150°E and 90°E, respectively. The convergence anomalies west of the date line almost coincide with positive OLR anomalies through all the composite phases.

An important feature of the vertical structure is that the upper-level divergence center overlies the center of convection and rising motion, while the low-level convergence center is either located at the leading edge of the convection region or there is significant low-level convergence in front of the convection center. The convection is situated in low-level westerlies with maximum westerly winds behind it. We wish to point out that the schematic structure described here is not always maintained through the entire life span, but it is typical especially at the strongest stage (phase 3, Fig. 7c).

6. Summary and discussions

This study documented the development and dynamic structure of tropical intraseasonal convection anomalies using 5-day mean anomalous OLR and ECMWF analyzed 200 and 850 mb wind data. The 5-day mean anomaly maps describe variations in a broad time scale from 10 to 90 days and a zonal scale roughly from wave 1 to 6. They carry signals of nonlinear evolution due to the interaction between motions with different time and spatial scales.

Some limitations arise due to the use of ECMWF wind data and a small sample for compositing. The quality of the ECMWF divergence field had been improved after September 1982 by adoption of nonlinear normal mode initialization scheme (Trenberth and Olson 1988). To check the possible impact of this inhomogeneity, we have examined another six-case composite (two strong and four moderate, all after September 1982 and during northern winter). The divergence patterns for post-September 1982 ECMWF data correspond qualitatively well with the present composite (figures are not shown). Some life-cycle details, however, seem to be sensitive to the specific cases comprising the composite. The anomalies on PMA maps carry signals of synoptic or subsynoptic scale higher frequency transients that occur sporadically within the envelope of the planetary scale low-frequency anomalies. This often causes irregularities in spatial and temporal domains and significant event-to-event variabilities. The composite structure of convection and circulation anomalies during the life cycle therefore gives only a gross qualitative picture of the mean behavior.

Based on the composite OLR anomalies for 36 events (Fig. 2), we propose a four-stage life cycle for intraseasonal convection anomalies: initiation, unstable intensification, maturity, and dissipation/emanation. Most low-frequency convection anomalies originate or become identifiable over equatorial Africa. Firm evidence of rapid intensification suggests that an

instability process is acting. The mature phase is characterized by a weakening in the maritime continent and redevelopment over the western Pacific. For moderate events the convection anomalies rapidly decay near the date line, while strong events dissipate further east in the central Pacific (150°W) and include an emanation of OLR anomalies, indicating tropical–extratropical interaction in the central and eastern Pacific.

This composite life cycle shows two essential observational features: the unstable growth in planetary-scale convective activity and their slow (5 m s^{-1}) eastward movement in the eastern hemisphere. In these regards, unstable feedback between the precipitational heating and equatorial Kelvin wave circulation provides an appealing interpretation (e.g., Lau and Peng 1987; Chang and Lim 1988; Wang 1988). The composite life cycle also suggests that the equatorial Indian Ocean is the most favorable geographic location for the development of low-frequency convection anomalies, and the western Pacific is a favorable location for reintensification. An explanation is needed to account for this geographic preference for the development. Besides the warm ocean surface condition, the interaction between Walker circulation and transient intraseasonal disturbance and the interaction between monsoon circulation and equatorial intraseasonal mode may be important factors in determining favored locations for development.

The triggering mechanisms for the formation and rapid amplification of large-scale low-frequency convection anomalies over equatorial Africa or the Indian Ocean are unclear. There are three possibilities. First, although convection anomalies are mainly confined to the eastern hemisphere, the upper tropospheric circulation anomalies may travel across the western hemisphere at a much higher speed, inducing a subsequent convection burst over the Indian Ocean. (See Figs. 5e–f, also Knutson et al. 1986; Lau and Peng 1987; Miyahara 1987.) Another possible triggering is due to active interaction between tropics and extratropics in phases 1 and 2. Strong equatorward meridional flow may activate equatorial convection in those regions (Figs. 6a, b, also Murakami 1987, 1988). Finally, as shown in Fig. 3, negative OLR anomalies tend to emanate from the equatorial central Pacific toward the extratropics of both hemispheres. Using analyses of four years of satellite-derived microwave radiance data, Gao and Stanford (1988) showed a possible propagation route from the central equatorial Pacific across lower South America and turning equatorward to the equatorial Indian Ocean. This possible energy exchange between extratropics and tropics can reinforce or generate convective disturbances over the Indian Ocean. The dissipation of convective activity near the date line most likely results from the rapid decrease of sea surface temperature (SST) to the east.

The vertical structure in equatorial zonal plane shows well-defined relationships among OLR, zonal wind and vertical motion anomalies (Fig. 7). There are three pronounced features. First, at the mature phase the upper-level divergence and the midtropospheric rising motion overlap the convection, while the lower-level convergence center is located at the leading edge of the convection region. In their analysis of the intraseasonal mode in an ideal general circulation model (GCM) with zonally symmetric climatology, Lau et al. (1988) made a composite structure of the intraseasonal mode based on primary EOF components that shows a westward tilt of the upward motion. Wang (1988) showed that this feature may be related to boundary layer frictional effects. Second, the amplitude of the zonal wind fluctuation at 200 mb is about twice that of 850 mb. This feature suggests the importance of the higher vertical modes in the interaction between the low-frequency wave and associated precipitational heating. The unstable interaction of the boundary layer frictional moisture convergence with condensational heating may account for this baroclinic vertical structure asymmetric with respect to the midtroposphere by means of coupling of vertical modes (Wang and Chen 1989). Finally, although 200 mb easterly anomalies and 850 mb westerly anomalies are coupled with equatorial convection in the eastern hemisphere, the phase speed of the wind anomalies exceeds that of convection. Therefore, the spatial phase relationship among OLR, 200 mb and 850 mb zonal wind anomalies change in the evolution process. From phase 1 to phase 3, 200 mb easterly and 850 mb westerly centers lag the equatorial convection center. This structure characterizes development of the convection. They are almost in phase with the convection at phase 5, and slightly lead the convection at phase 6, a decoupled situation. Observed negative OLR anomalies in most of the life cycle nearly coincide with low-level westerly and upper-level easterly anomalies. This feature has not been properly modeled and interpreted. To date, all theoretical models for intraseasonal oscillations yield a baroclinic wind anomaly whose phase is in quadrature with the vertical motion (OLR) anomaly.

Comparison of OLR and horizontal wind anomalies also reveals good coherence. At upper (lower) levels, two anticyclonic (cyclonic) systems reside north and south of the equatorial convection anomaly, respectively. Easterlies between two upper-level anticyclonic cells and westerlies between two lower-level cyclonic cells are coupled with the equatorial convection, and propagate eastward (Figs. 5 and 6). Schematic diagrams of the dynamic structure of transient intraseasonal OLR anomalies are highlighted in Fig. 8 for phases 3 and 5, respectively. When the convection anomaly is over the Indian Ocean (phase 3), to the east of the enhanced convection region significant westerly anomalies at 200 mb are associated with two subtropical cyclones, while strong easterlies at 850 mb are in between two anticyclonic ridges extending from

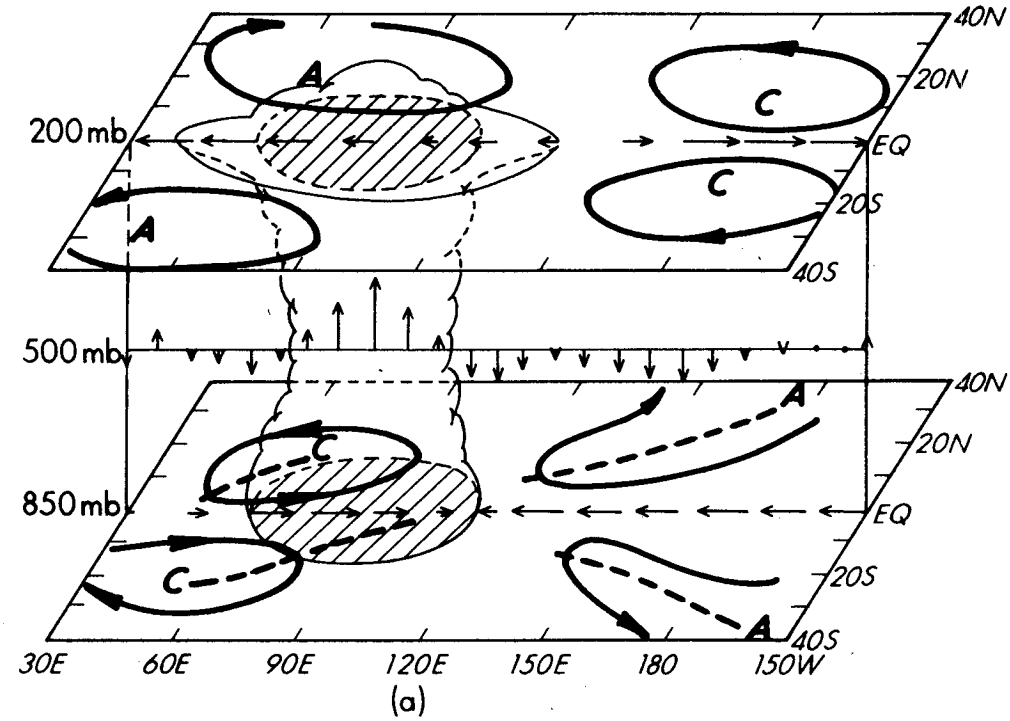

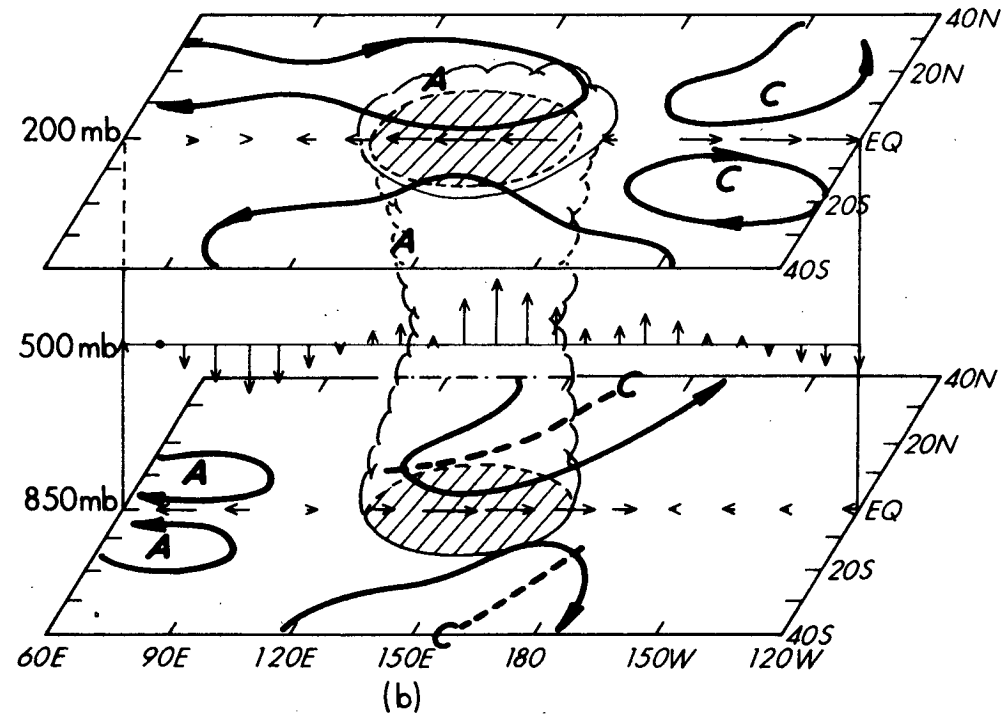

FIG. 8. Schematic depiction of the characteristic structure of the intraseasonal low-frequency waves at (a) phase 3, and (b) phase 5. The shaded regions correspond to areas where OLR anomalies are less than -7.5 W m^{-2} in Figs. 3c, e. The zonal wind and vertical velocity anomalies in the equatorial zonal plane are the same as those in Figs. 7c, e except the scaling. Bold letters A and C represent anticyclonic and cyclonic circulation centers. The circulation cells highlight characteristic wind anomalies associated with the convection anomalies in Figs. 5c, e and Figs. 6c, e.

two midlatitude anticyclones (Fig. 8a). On the other hand, when the convection region reaches the western Pacific (phase 5), while the 200 mb westerly anomalies and associated twin cyclones remain east of the convection region, the 850 mb easterly anomalies in front of the convection disappear. Meanwhile, weak 850 mb equatorial easterly anomalies and associated twin anticyclones develop west of the convection region over the Indian Ocean. In fact, after the convection anomaly passes the western Pacific, both the convection anomalies and the low-level circulation anomalies dissipate but the circulation anomalies at upper troposphere continue to traverse the Pacific basin (Figs. 5f, g). This provides evidence that only the upper tropospheric circulation anomalies can maintain a longer period and propagate downstream after the convection dies out in the central Pacific. Previous studies suggested that these upper tropospheric circulation anomalies appear to travel across the entire western hemisphere (e.g., Lorenc 1984; Knutson et al. 1986).

The composite horizontal structure indicates that the intraseasonal disturbances are characterized by strong coupling between the equatorial zonal wind anomalies and subtropical cyclonic or anticyclonic cells. These disturbances appear to involve a coupling between moist Kelvin and Rossby modes. A simple theoretical analysis has demonstrated that a unified boundary layer moisture convergence generated by both Kelvin and long Rossby mode of low meridional index could favor the intensification of the modified Kelvin mode, slow down its eastward propagation, and change its structure by creating significant meridional flow, while suppressing the growth of the modified Rossby mode (Wang and Rui 1989). Yet the coupled unstable mode remains trapped near the equator failing to couple with subtropical rotational cells. The discrepancy between theories and observations regarding the horizontal and vertical structures reveals a major defect of the current theories.

Acknowledgments. Dr. T. Murakami made his OLR data and ECMWF wind data available to us. The comments of Drs. T. Murakami and T. A. Schroeder and of the anonymous reviewers are gratefully acknowledged. This research was supported by NOAA Grant NA 85 ABH00032 and by NSF Grant ATM-8814626.

REFERENCES

Chang, C.-P., and H. Lim, 1988: Kelvin wave-CISK: A possible mechanism for the 30–50 day oscillation. *J. Atmos. Sci.*, **45**, 1709–1720.

Gao, X. H., and J. L. Stanford, 1988: Possible feedback path for low-frequency atmospheric oscillation. *J. Atmos. Sci.*, **45**, 1425–1432.

Krishnamurti, T. N., P. K. Jayakumar, J. Shen, N. Surgi and A. Kumar, 1985: Divergent circulations on the 30 to 50 day time scale. *J. Atmos. Sci.*, **42**, 364–375.

Knutson, T. R., and K. M. Weickmann, 1987: 30–60 day atmospheric oscillation: composite life cycles of convection and circulation anomalies. *Mon. Wea. Rev.*, **115**, 1407–1436.

——, —— and J. E. Kutzbach, 1986: Global-scale intraseasonal oscillation of outgoing longwave radiation and 200 mb zonal wind during Northern Hemisphere summer. *Mon. Wea. Rev.*, **114**, 605–623.

Lau, K.-M., and L. Peng, 1987: Origin of the low frequency (intraseasonal) oscillation in the tropical atmosphere. *J. Atmos. Sci.*, **44**, 950–972.

Lau, N.-C., I. M. Held and J. D. Neelin, 1988: The Madden–Julian oscillation in an idealized general circulation model. *J. Atmos. Sci.*, **45**, 3810–3812.

Liebmann, B., 1987: Observed relationships between large-scale tropical convection and the tropical circulation on subseasonal time scales during Northern Hemisphere winter. *J. Atmos. Sci.*, **44**, 2543–2561.

Lorenc, A. C., 1984: The evolution of planetary scale divergence during the FGGE year. *Quart. J. Roy. Meteor. Soc.*, **110**, 427–444.

Madden, R. A., 1986: Seasonal variation of the 40–50 day oscillation in the tropics. *J. Atmos. Sci.*, **43**, 3138–3158.

——, and P. R. Julian, 1972: Description of global-scale circulation cell in the tropics with a 40–50 day period. *J. Atmos. Sci.*, **29**, 1109–1123.

Miyahara, S., 1987: A simple model of the tropical intraseasonal oscillation. *J. Meteor. Soc. Japan*, **65**, 341–351.

Murakami, T., 1987: Intraseasonal atmospheric teleconnection patterns during the Northern Hemisphere summer. *Mon. Wea. Rev.*, **115**, 2134–2144.

——, 1988: Intraseasonal atmospheric teleconnection patterns during the Northern Hemisphere winter. *J. Climate.*, **1**, 117–131.

Rosenlof, K. H., D. E. Stevens, J. R. Anderson and P. E. Ciesielski, 1986: The Walker circulation with observed zonal winds, a mean Hadley cell, and cumulus friction. *J. Atmos. Sci.*, **43**, 449–467.

Trenberth, K. E., and J. G. Olson, 1988: An evaluation and intercomparison of global analyses from the National Meteorological Center and the European Centre for Medium Range Weather Forecasts, *Bull. Amer. Meteor. Soc.*, **69**, 1047–1057.

Wang, B., 1988: Dynamics of tropical low-frequency waves: An analysis of the moist Kelvin wave. *J. Atmos. Sci.*, **45**, 2051–2065.

——, and J.-K. Chen, 1989: On the zonal scale selection and vertical structure of the equatorial intraseasonal waves. To appear in *Quart. J. Roy. Meteor. Soc.*, **115**, in press.

——, and H. Rui, 1989: Dynamics of the coupled moist Kelvin-Rossby wave on an equatorial beta-plane, *J. Atmos. Sci.*, in press.

Wang, X.-L., and T. Murakami, 1988: Intraseasonal disturbance activity before, during and after the 1982–83 ENSO. *J. Atmos. Sci.*, **45**, 3754–3770.

Weickmann, K. M., G. R. Lussky and J. E. Kutzbach, 1985: Intraseasonal (30–60) fluctuations of outgoing longwave radiation and 250 mb streamfunction during northern winter. *Mon. Wea. Rev.*, **113**, 941–960.